

Theoretical Investigation of Excitonic Gain in ZnO–Mg_xZn_{1–x}O Strained Quantum Wells

A. P. Abiyasa, S. F. Yu, *Senior Member, IEEE*, W. J. Fan, and S. P. Lau

Abstract—Free-excitonic gain of wurtzite ZnO–Mg_xZn_{1–x}O quantum wells (QWs) is studied theoretically. The valence band structure of ZnO–Mg_xZn_{1–x}O QWs with the consideration of biaxial strain and exciton–phonon interaction is calculated based on a 6×6 Hamiltonian. From the available experimental data, the band offset ratio and conduction band deformation potential of ZnO–Mg_xZn_{1–x}O QWs are found to be 60/40 and –6.8 eV, respectively. The influence of biaxial strain on the peak free-excitonic gain of ZnO–Mg_xZn_{1–x}O QWs for various well-width and mole fraction of Mg is also investigated.

Index Terms—Excitonic gain, numerical modeling, quantum wells (QWs), zinc oxide.

I. INTRODUCTION

DUE TO their large excitonic transition energy (~ 3.34 eV) and binding energy (~ 60 meV) [1], ZnO materials have drawn considerable attention for the application in ultraviolet optoelectronics. Further improvements on these excitonic characteristics of bulk ZnO materials is possible if ZnO-based quantum-well (QW) structures are constructed. Recently, investigations on the excitonic characteristics of ZnO–Mg_xZn_{1–x}O QWs growth on ScAlMgO₄ substrate have reported the enhancement of excitonic transition energy (> 3.6 eV) as well as the reduction of excitation threshold (≤ 17 kW/cm²) [2]. Physical models, inclusive of the influence of exciton–phonon interaction as formulated by Pollmann–Büttner potential [3], have been developed to interpret the excitonic transition characteristics of ZnO–Mg_xZn_{1–x}O QWs [4]. Furthermore, spontaneous and piezoelectric polarization effects have been taken into calculations of the optical characteristics of ZnO–Mg_xZn_{1–x}O QWs [5], [6]. Nevertheless, to the best of our knowledge, there is little report on the theoretical study of the free-excitonic gain of ZnO–Mg_xZn_{1–x}O QWs especially with the influence of exciton–phonon interaction. It is also desirable to analyze the design of ZnO QWs for maximum free-excitonic gain in order to realize efficient excitonic lasing.

In this paper, the influence of biaxial strain and exciton–phonon interaction on the free-excitonic gain of wurtzite ZnO–Mg_xZn_{1–x}O QWs for various well-width and mole fraction of Mg is investigated theoretically. Two physical pa-

rameters, the band offset ratio and conduction band deformation potential, required for the calculation of the free-excitonic gain is also deduced from the available experimental data.

This paper is organized as follows. In Section II, the conduction and valence band structures of the ZnO QWs are modeled by a parabolic band model and a 6 × 6 strained Hamiltonian, respectively. The effective mass parameters of the strained Hamiltonian are deduced from the empirical pseudopotential method (EPM). The electron and hole wave functions are approximated by plane-wave expansion method [7]. Free-exciton energy of ZnO–Mg_xZn_{1–x}O QWs is then deduced by variational method with exciton–phonon interaction taken into consideration. The corresponding momentum matrix elements and the free-exciton optical gain of the ZnO QWs are, therefore, calculated. In Section III, the valence energy dispersion of ZnO–Mg_xZn_{1–x}O QWs is deduced and the importance of the inclusion of A-, B- and C- holes states for the study of exciton states is then discussed. The calculated excitonic transition energy of the ZnO–Mg_xZn_{1–x}O QWs is subsequently compared with the experimental results for validation purposes. Hence, the band offset ratio and conduction band deformation potential are estimated for the calculation of free-excitonic gain. Furthermore, the optimum design of the optical gain of ZnO–Mg_xZn_{1–x}O QWs under the influence of biaxial strain is investigated. Section IV concludes the results obtained.

II. THEORY

In this section, the energy bands of ZnO–Mg_xZn_{1–x}O QWs are modeled, with the assumption that the conduction and valence bands are decoupled, by using the $\mathbf{k} \cdot \mathbf{p}$ method. A single parabolic band model is used to approximate the conduction band. For the valence band, a 6×6 strained Hamiltonian is used to account for spin-orbit coupling which result in degenerate A-, B- and C-hole bands [8]. A center mass coordinate system is applied to form the exciton Hamiltonian at Γ point with the consideration of exciton–phonon interaction represented by Pollmann–Büttner potential. The exciton ground state energy is then deduced by using the variational method. The numerical model for the calculation of the optical gain of the ZnO–Mg_xZn_{1–x}O QWs for the bound and continuum state excitons is, therefore, established.

Fig. 1 shows the schematic of the wurtzite ZnO–Mg_xZn_{1–x}O QWs used in the model. If the z axis is assumed to be along the growth direction, the wave function $\psi_{n,k}^c(z)$ for the electron can be written as [9]

$$\psi_{n,k}^c(z) = \sum_{\eta=\uparrow,\downarrow} \varphi_n(z, \mathbf{k}) |S, \eta\rangle \quad (1)$$

Manuscript received December 4, 2005; revised January 15, 2006. This work was supported in part by the Agency for Science, Technology, and Research of Singapore under Project 022-101-0033 and in part by the Nippon Sheet Glass Foundation.

The authors are with the School of Electrical and Electronic Engineering, Nanyang Technological University, Singapore 639798 (e-mail: esfyu@ntu.edu.sg).

Digital Object Identifier 10.1109/JQE.2006.872318

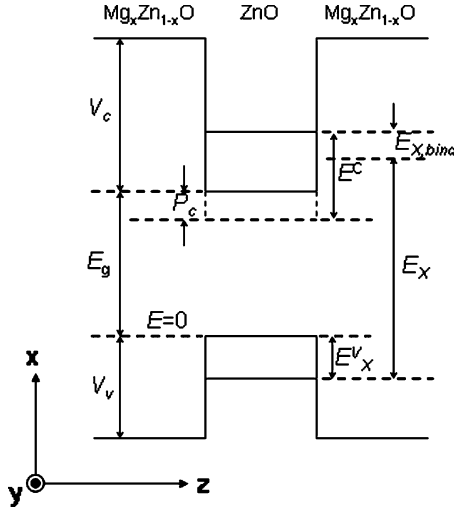


Fig. 1. Schematic of a ZnO–Mg_xZn_{1–x}O QW with the lowest energy subbands. Excitons transition energy, E_X (where $X = A, B, \text{ or } C$) and binding energy, $E_{X,\text{bind}}$ are shown in the figure.

where n indexes the number of conduction subbands, η is electron spin, $|S, \eta\rangle$ is the Bloch function transforming like s-state atomic wavefunctions, and \mathbf{k} is the wave vector. Using plane-wave expansion, the normalized envelope function can be written as

$$\varphi_n(z, \mathbf{k}) = e^{i(k_x x + k_y y)} \sum_p g_{n,p,k_x,k_y} \cdot \frac{1}{\sqrt{L}} e^{i(k_z + p \cdot \frac{2\pi}{L})z} \quad (2)$$

where $i = \sqrt{-1}$, $L = L_w + L_b$, L_w is the well width of the QW, L_b is the width of the barrier region, and p is an integer running through the plane-waves that construct the z -dependent envelope function. The eigen-equation of electron envelope function can be expressed as

$$(H^c + V_c(z)) \varphi_n(z, \mathbf{k}) = E_n^c(\mathbf{k}) \varphi_n(z, \mathbf{k}) \quad (3)$$

where $H^c = (1/2)\hbar^2((k_x^2 + k_y^2)/m_e^{\parallel} + k_z^2/m_e^{\perp}) + P_c(z)$ and $V_c(z)$ is the QW's profile of the unstrained conduction band energy. m_e^{\parallel} and m_e^{\perp} are the electron effective masses parallel and perpendicular to the in-plane direction, respectively, and \hbar is the Planck's constant. The hydrostatic deformation potential term, $P_c(z)$, is assumed equal to $P_c(z) = a^c(\varepsilon_{xx} + \varepsilon_{yy} + \varepsilon_{zz})$ inside the well region and $P_c(z) = 0$ inside the barrier region. a^c is the conduction band deformation potential constant to be determined. If the barrier width of the QWs is large, the energy dispersion $E_n^c(\mathbf{k})$ in the calculation can be approximated by $E_n^c(k_x, k_y)$ as the dependence of $E_n^c(\mathbf{k})$ on k_z is insignificant.

Based on a 6×6 Hamiltonian, the QWs valence holes state can be described by [9], [10]

$$\psi_{m,k}^v(z) = \sum_{j=1-6} \phi_m^{(j)}(z, \mathbf{k}) |u_j\rangle. \quad (4)$$

The basis set $|u_{1-6}\rangle$, for the valence bands are chosen to be

$$\begin{aligned} |u_1\rangle &= -\frac{1}{\sqrt{2}}|X + iY, \uparrow\rangle & |u_2\rangle &= \frac{1}{\sqrt{2}}|X - iY, \uparrow\rangle \\ |u_3\rangle &= |Z, \uparrow\rangle & |u_4\rangle &= \frac{1}{\sqrt{2}}|X - iY, \downarrow\rangle \\ |u_5\rangle &= -\frac{1}{\sqrt{2}}|X + iY, \downarrow\rangle & |u_6\rangle &= |Z, \downarrow\rangle \end{aligned} \quad (5)$$

where $|X\rangle$, $|Y\rangle$, and $|Z\rangle$, are the Bloch functions at the Γ point transforming like the p_x , p_y , and p_z atomic wavefunctions, respectively. The envelope function of valence band holes of the QWs is evaluated by diagonalizing

$$\sum_{j=1}^6 (H_{j'j}^v + \delta_{j'j} V_v(z)) \phi_m^{(j)}(z, \mathbf{k}) = E_m^v(z, \mathbf{k}) \phi_m^{(j')}(z, \mathbf{k}) \quad (6)$$

where $j' = 1, 2, \dots, 6, m$ indexes the valence subbands and $V_v(z)$ is the potential profile of the unstrained valence-band energy. Strain-induced band-edge shifts in the well are accounted in the diagonal terms of the Hamiltonian $H_{jj'}^v$. The six-dimensional envelope functions $\phi_m^{(j)}(z, \mathbf{k})$ are described by

$$\phi_m^{(j)}(z, \mathbf{k}) = e^{i(k_x x + k_y y)} \sum_p a_{m,p,k_x,k_y}^{(j)} \frac{1}{\sqrt{L}} e^{i(k_z + p \cdot \frac{2\pi}{L})z}. \quad (7)$$

The 6×6 Hamiltonian of the valence bands for wurtzite semiconductor including strain effect is given by [9], [10]

$$H_{6 \times 6}^v = \begin{bmatrix} F & -K^* & -H^* & 0 & 0 & 0 \\ -K & G & H & 0 & 0 & \Delta \\ -H & H^* & \lambda & 0 & \Delta & 0 \\ 0 & 0 & 0 & F & -K & H \\ 0 & 0 & \Delta & -K^* & G & -H^* \\ 0 & \Delta & 0 & H^* & -H & \lambda \end{bmatrix} \quad (8)$$

where

$$\begin{aligned} F &= \Delta_1 + \Delta_2 + \lambda + \theta, & G &= \Delta_1 - \Delta_2 + \lambda + \theta, & \Delta &= \sqrt{2}\Delta_3 \\ \lambda &= \frac{\hbar^2}{2m_0} [A_1 k_z^2 + A_2 (k_x^2 + k_y^2)] + D_1 \varepsilon_{zz} + D_2 (\varepsilon_{xx} + \varepsilon_{yy}) \\ \theta &= \frac{\hbar^2}{2m_0} [A_3 k_z^2 + A_4 (k_x^2 + k_y^2)] + D_3 \varepsilon_{zz} + D_4 (\varepsilon_{xx} + \varepsilon_{yy}) \\ K &= \frac{\hbar^2}{2m_0} A_5 (k_x + ik_y)^2 + D_5 \varepsilon_+ \\ H &= \frac{\hbar^2}{2m_0} A_6 (k_x + ik_y) k_z + D_6 \varepsilon_{z+}. \end{aligned} \quad (9)$$

In (9), Δ_1 is the crystal field split energy, Δ_2 and Δ_3 account for the spin-orbit interaction, ε_{ij} is an element of the strain tensor, $\varepsilon_+ = \varepsilon_{xx} + 2i\varepsilon_{xy} - \varepsilon_{yy}$, $\varepsilon_{z+} = \varepsilon_{xx} + i\varepsilon_{yz}$, A_{1-6} are the effective-mass parameters, and D_{1-6} are the deformation potentials. For biaxial strained QWs, the strain tensor in the well region comprises of $\varepsilon_{xx} = \varepsilon_{yy} = (a_0 - a)/a$, $\varepsilon_{zz} = -2C_{13}\varepsilon_{xx}/C_{33}$

and $\varepsilon_{xy} = \varepsilon_{yz} = \varepsilon_{zx} = 0$, where a_0 and a are the lattice constants of the MgZnO barrier and ZnO well layers, respectively. C_{13} and C_{33} are the stiffness constants of the ZnO well layer.

In ZnO bulk and QWs materials, the interaction between exciton and phonon is significant. It has been shown that the exciton binding energy in ZnO–Mg_xZn_{1-x}O QWs is greatly enhanced by exciton–phonon interaction [4]. This is because the strong confinement of longitudinal phonons enhances the coupling between excitons and phonons inside the QWs. However, the analysis of exciton–phonon coupling in QWs using three phonon modes (i.e., at the well, barrier and their interface) is very complicated [11]. Therefore, we simplified the calculation by considering the exciton–bulk phonon interaction to approximate the total interaction of exciton with all the phonon modes [12], [13]. This is possible because the exciton–bulk phonon interaction can be correctly described by the Coulomb interaction using the Pollmann–Büttner potential [3].

Based on the above assumption, the exciton Hamiltonian, H_X , in the center mass coordinate system at the Γ point is given by [14], [15]

$$H_X = H_e + H_h - \frac{\hbar^2 \nabla_\rho^2}{2\mu} + V_{PB} \quad (10)$$

where $H_e (= H^c + V_c)$ and $H_h (= H^v + V_v)$ are the electron and hole Hamiltonians at the Γ point, respectively, without Coulomb interaction. The third term on the right-hand-side of (10) represents the kinetic energy of electrons and holes. V_{PB} , which takes into account of the exciton–phonon interaction, is the Pollmann–Büttner potential. V_{PB} can be written explicitly as [3]

$$V_{PB}(r) = -\frac{e^2}{4\pi\varepsilon_s\varepsilon_0 r} - \frac{e^2}{4\pi\varepsilon_0 r} \left(\frac{1}{\varepsilon_\infty} - \frac{1}{\varepsilon_s} \right) \\ \times \left[\frac{C^4}{B^4} - \frac{m_e h_1}{\Delta m} e^{-\frac{rA_1}{R_1}} + \frac{m_h h_2}{\Delta m} e^{-\frac{rA_2}{R_2}} \right. \\ \left. - \left(h_\mu + \frac{C^3 r}{2B^3 a_{exc}} \right) e^{-\frac{rB}{R_\mu}} \right] \quad (11)$$

$$R_1 = \sqrt{\frac{\hbar}{2m_e\omega}} \quad R_2 = \sqrt{\frac{\hbar}{2m_h\omega}} \quad R_\mu = \sqrt{\frac{\hbar}{2\mu\omega}} \\ A_1^2 = 1 + \frac{R_1^2}{a_{exc}^2} \quad A_2^2 = 1 + \frac{R_2^2}{a_{exc}^2} \\ B^2 = 1 + \frac{R_\mu^2}{a_{exc}^2} \quad C^2 = \frac{R_\mu^2}{a_{exc}^2} \\ h_1 = 1 + \left(\frac{m_h R_1}{m_e a_{exc}} \right)^2 \quad h_2 = 1 + \left(\frac{m_e R_2}{m_h a_{exc}} \right)^2 \\ h_\mu = \frac{C^4}{B^4} - \left(\frac{m_e}{m_h} + \frac{m_h}{m_e} \right) C^2 \\ \Delta m = m_h - m_e \quad r = \sqrt{(z_e - z_h)^2 + \rho^2} \quad (12)$$

where m_e is the bulk electron effective mass, m_h (for A-, B-, or C- valence bands) is the bulk hole effective mass, μ is the bulk exciton reduced effective mass, and a_{exc} is the bulk exciton Bohr's radius. $\varepsilon_s (= 8.1)$ is the static dielectric constant,

$\varepsilon_\infty (= 4.0)$ is the high frequency dielectric constant and $\hbar\omega (= 72 \text{ meV})$ is the LO phonon energy [4].

For anisotropic crystal like ZnO, we can relate the effective mass parameters and the holes effective masses for the parallel and perpendicular effective mass to the in-plane direction as follows [16]:

$$m_A^\parallel = -(A_2 + A_4 + A_5)^{-1} \quad m_A^\perp = -(A_1 + A_3)^{-1} \\ m_B^\parallel = -(A_2 + A_4 - A_5)^{-1} \quad m_B^\perp = -(A_1 + A_3)^{-1} \\ m_C^\parallel = -A_2^{-1} \quad m_C^\perp = -A_1^{-1}. \quad (13)$$

It is noted that the effective masses of A- and B- holes given in (13) are different from that in [16]. This is because the arrangement of the valence bands symmetry of A- and B-holes in ZnO is in reverse order to that of the GaN. The exciton reduced effective mass in the direction parallel (perpendicular) to the in-plane direction is given as $1/\mu_i^\parallel (\mu_i^\perp) = (1/m_e^\parallel (m_e^\perp)) + (1/m_{h,i}^\parallel (m_{h,i}^\perp))$, where $m_e^\parallel (m_e^\perp)$ is the parallel (perpendicular) electron effective mass, $m_{h,i}^\parallel (m_{h,i}^\perp)$ is the parallel (perpendicular) holes effective mass and $i = A, B$, or C. Hence, the bulk exciton reduced effective mass is then given as $\mu_i = \sqrt{\mu_i^\parallel \mu_i^\perp}$ [17] and the bulk exciton Bohr's radius can be written as $a_{exc}^i = 4\pi\varepsilon_s\varepsilon_0\hbar^2/e^2\mu_i$ for the i th excitons. The bulk electron and holes effective masses are then given by $m_e = \sqrt{m_e^\parallel m_e^\perp}$ and $m_{h,i} = \sqrt{m_{h,i}^\parallel m_{h,i}^\perp}$, respectively.

As the optical properties of ZnO materials are determined by the optical transition at the center of Brillouin zone Γ the free-exciton states at Γ point can be analyzed by variational method. This can be done by using a trial function, Ψ [14], [15]

$$\Psi = \varphi_n(z)\phi_m(z)\psi(\rho), \quad (14)$$

$$\psi(\rho) = \left(\frac{2}{\pi} \right)^{\frac{1}{2}} \frac{1}{\lambda} \exp\left(-\frac{\rho}{\lambda}\right) \quad (15)$$

where $\varphi_n(z)$ and $\phi_m(z)$ are the electron and hole envelope functions, respectively, without Coulomb interaction. $\psi(\rho)$ is the trial wavefunction for 1-s bound exciton, ρ is the in-plane coordinate, and λ is the trial parameter. If the exciton transition energy $E_X(\lambda)$ can be minimized with suitable selection of λ using [14], [15]

$$E_X(\lambda) = \min \frac{\langle \Psi | H_X | \Psi \rangle}{\langle \Psi | \Psi \rangle} \\ = (E_g + P_c) + E_n^c(0) + E_m^v(0) + E_{X,\text{bind}}(\lambda) \quad (16)$$

we can deduce the realistic value of E_X . In (16), E_g is the bandgap of ZnO well, $E_n^c(0)$ and $E_m^v(0)$ are the eigenvalues of conduction and valence bands at Γ point, respectively, and $E_{X,\text{bind}}(\lambda)$ is the binding energy calculated by the variational method. The binding energy of different X (related to A, B, or C hole bands) corresponds to the ground state energy of A-, B- or C-excitons.

To calculate the excitonic gain, we assumed that the total optical gain of the ZnO QWs is contributed by the bound exciton and continuum states. We can calculate the bound exciton states by using the variational method. For the continuum states, the calculation is assumed to be similar to that of the band-to-band transition calculation with the inclusion of Sommerfeld's enhancement factor. The momentum matrix element for the band-to-band transition of ZnO QWs is given by [9]

$$\mathbf{M}_{nm}(k_x, k_y) = \left\langle \psi_{m,k_x,k_y}^v | \hat{p} | \psi_{n,k_x,k_y}^c \right\rangle \quad (17)$$

where we have neglected the dispersion in the k_z direction. The momentum matrix can be resolved into TE polarization and can be written as

$$\begin{aligned} \hat{x} \cdot \mathbf{M}_{nm}(k_x, k_y) &= \left\langle \psi_{m,k_x,k_y}^v | \hat{p}_x | \psi_{n,k_x,k_y}^c \right\rangle \\ &= \langle S | \hat{p}_x | X \rangle \\ &\cdot \sum_p \frac{1}{\sqrt{2}} \left(-a_{m,p,k_x,k_y}^1 + a_{m,p,k_x,k_y}^2 \right. \\ &\quad \left. + a_{m,p,k_x,k_y}^4 - a_{m,p,k_x,k_y}^5 \right) g_{n,p,k_x,k_y}^*. \end{aligned} \quad (18)$$

For TM polarization, the momentum matrix can be expressed as

$$\begin{aligned} \hat{z} \cdot \mathbf{M}_{nm}(k_x, k_y) &= \left\langle \psi_{m,k_x,k_y}^v | \hat{p}_z | \psi_{n,k_x,k_y}^c \right\rangle \\ &= \langle S | \hat{p}_z | Z \rangle \cdot \sum_p \left(a_{m,p,k_x,k_y}^3 + a_{m,p,k_x,k_y}^6 \right) g_{n,p,k_x,k_y}^*. \end{aligned} \quad (19)$$

In (18) and (19), the band-edge momentum matrix elements, $\langle S | \hat{p}_x | X \rangle$ and $\langle S | \hat{p}_z | Z \rangle$ for the wurtzite structure, are given as [10]

$$\begin{aligned} &|\langle S | \hat{p}_x | X \rangle|^2 \\ &= \frac{m_0}{2} \left(\frac{m_0}{m_e^{\parallel}} - 1 \right) \frac{E_g [(E_g + \Delta_1 + \Delta_2)(E_g + 2\Delta_2) - 2\Delta_3^2]}{(E_g + \Delta_1 + \Delta_2)(E_g + \Delta_2) - \Delta_3^2} \end{aligned} \quad (20)$$

$$\begin{aligned} &|\langle S | \hat{p}_z | Z \rangle|^2 \\ &= \frac{m_0}{2} \left(\frac{m_0}{m_e^{\perp}} - 1 \right) \frac{[(E_g + \Delta_1 + \Delta_2)(E_g + 2\Delta_2) - 2\Delta_3^2]}{(E_g + 2\Delta_2)}. \end{aligned} \quad (21)$$

Hence, the excitonic gain of the bound exciton states g_{bound} at Γ point can be expressed as [18], [19]

$$\begin{aligned} g_{\text{bound}}(E) &= \frac{2e^2\pi\hbar}{n_r c \varepsilon_0 m_0^2 L_w E} \left| \sum_X \psi_X(\rho=0) I_{nm} \hat{e} \cdot \mathbf{M}_{nm}(0) \right|^2 \\ &\times \frac{1}{\pi} \frac{\frac{\hbar}{\tau}}{(E_X - E)^2 + (\frac{\hbar}{\tau})^2} (f_n^c + f_m^v - 1) \end{aligned} \quad (22)$$

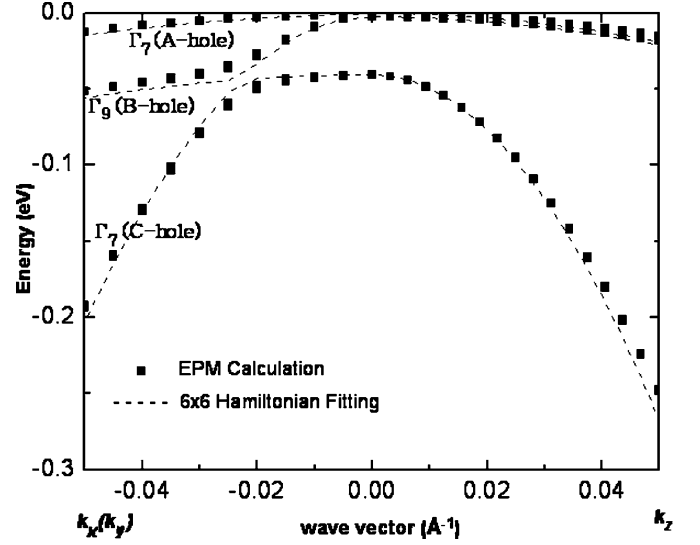


Fig. 2. ZnO valence bands computed by EPM (solid squares) and 6×6 Hamiltonian (dashed lines) calculation for the case without biaxial strain. The three hole-bands, which are A-state (Γ_7 symmetry), B-state (Γ_9 symmetry) and C-state (Γ_7 symmetry), are indicated from top to bottom.

and that of the continuum states g_{cont} is given by

$$\begin{aligned} g_{\text{cont}}(E) &= \frac{e^2\pi\hbar}{n_r c \varepsilon_0 m_0^2 L_w E} S(E) \\ &\times \sum_{nm} \iint \frac{dk_x dk_y}{(2\pi)^2} |\hat{e} \cdot \mathbf{M}_{nm}(k_x, k_y)|^2 \\ &\times \frac{1}{\pi} \frac{\frac{\hbar}{\tau}}{(E_{nm} - E)^2 + (\frac{\hbar}{\tau})^2} (f_n^c + f_m^v - 1) \end{aligned} \quad (23)$$

where n_r ($= 2.1$) is the refractive index of ZnO, c is the speed of light in free space, ε_0 is free space permittivity, e is the electron charge, and E_{nm} is the band-to-band transition energy equal to $E_{nm}(k_x, k_y) = (E_g + P_c) + E_n^c(k_x, k_y) + E_m^v(k_x, k_y)$. I_{nm} is the overlap integral for electron and hole, \hat{e} is the electric field polarization vector (TE or TM) and $S(E)$ is the Sommerfeld's enhancement factor [18]. Comparing to [19], our expression of optical gain in the continuum states gain is differed by a Sommerfeld's enhancement factor. To account of the broadening effect, we have assumed a Lorentzian function with broadening lifetime τ of 0.1 ps. The expression of Fermi function for electron f_n^c and that for hole, f_m^v can be obtained from [9].

III. RESULTS AND DISCUSSIONS

In this section, the ZnO valence bands structure is calculated using EPM. Effective mass parameters are then extracted from the fitting to the EPM results. The values of the band-offset ratio and conduction band deformation potential of ZnO-Mg_xZn_{1-x}O QWs are estimated from available experimental data. The oscillator strength of the ZnO-Mg_xZn_{1-x}O QWs is also maximized by varying the width of the QWs. Hence, the optimum design of the ZnO QWs can be deduced with the appropriate mole fraction of Mg.

Fig. 2 shows the valence band structure of ZnO materials obtained from EPM calculation. The ordering of ZnO valence

TABLE I
PARAMETERS LIST FOR THE CALCULATION OF THE EXCITONIC GAIN OF ZnO–Mg_xZn_{1-x}O QWS

Parameters	ZnO	Mg _x Zn _{1-x} O
Lattice constant (Å)		
<i>a</i>	3.250 [25]	3.250 + 0.036 <i>x</i> [25]
<i>c</i>	5.213 [25]	–
Energy parameters		
<i>E_g</i> (eV) @ 300 K	3.42 [26]	3.42+2.00 <i>x</i> [26]
Δ_1 (=Δ _{cr}) (meV)	39.10 (our work)	–
Δ _{so} (meV)	–3.50 (our work)	–
Δ ₂ = Δ ₃ =Δ _{so} /3 (meV)	–1.17 (our work)	–
Conduction-band effective mass (<i>m</i> ₀)		
<i>m_e</i>	0.24 [8]	
<i>m_e[⊥]</i>	0.24 [8]	
Valence-band effective mass parameters		
<i>A</i> ₁	–6.68036 (our work)	
<i>A</i> ₂	–0.45388 (our work)	
<i>A</i> ₃	–6.12750 (our work)	
<i>A</i> ₄	–2.70374 (our work)	
<i>A</i> ₅	–2.76690 (our work)	
<i>A</i> ₆	–4.62566 (our work)	
Deformation potentials (eV)		
<i>D</i> ₁	–2.66 [27]	
<i>D</i> ₂	2.82 [27]	
<i>D</i> ₃	–1.34 [27]	
<i>D</i> ₄	1.00 [27]	
<i>D</i> ₅	0.00	
<i>D</i> ₆	0.00	
Elastic stiffness constants (GPa)		
<i>C</i> ₁₃	105.1 [28]	
<i>C</i> ₃₃	210.9 [28]	
Holes effective mass (<i>m</i> ₀)		
<i>m_A</i>	0.17 (our work)	
<i>m_A[⊥]</i>	1.81 (our work)	
<i>m_B</i>	2.56 (our work)	
<i>m_B[⊥]</i>	1.81 (our work)	
<i>m_C</i>	2.20 (our work)	
<i>m_C[⊥]</i>	0.15 (our work)	

band symmetry is assigned to be A-state (Γ_7 symmetry), B-state (Γ_9 symmetry), and C-state (Γ_7 symmetry) in descending order [20]. This assignment of states differs from the usual GaN wurtzite crystals (i.e., A- and B- states have Γ_9 and Γ_7 symmetries, respectively). This is because the presence of ZnO 3*d* band induces negative spin-orbit split-off energy in ZnO [8]. The symmetry at the valence band edge in the spin-orbit coupled states is defined by the Bloch basis function, $|u_j\rangle$ ($j = 1, 2, \dots, 6$). Based on these basis functions, the A- and C- states are formed by a mixture of $|u_2\rangle$ and $|u_3\rangle$ states ($|u_5\rangle$ and $|u_6\rangle$ states for the degenerate state) whereas the B-state is only composed of the $|u_1\rangle$ ($|u_4\rangle$) state. The difference between the A- and C-states is that the A-state is dominated by $|u_2\rangle$ ($|u_5\rangle$) state whereas the C-state is comprised mostly of $|u_3\rangle$ ($|u_6\rangle$) state. These different compositions, as shown later, affect the exciton's optical transition polarization properties formed by the conduction band electron with the A-, B-, or C- holes states due to the symmetry of the wavefunctions properties.

The effective mass parameters can be extracted from the EPM calculation of the valence band structures by using least square fitting method. We adjust the 6×6 Hamiltonian effective mass parameters to obtain the best-fitted results without biaxial strain

taken into consideration. Fig. 2 shows the fitting of the valence band structures and the deduced effective mass parameters, together with other parameters used for the calculations are listed in Table I. Our calculation of the effective mass parameters is in agreement with previously reported results [8].

We analyze the exciton transition energy of ZnO–Mg_xZn_{1-x}O QWs by the variational method. As mentioned in [4], the effect of exciton–phonon coupling in ZnO gives a more accurate calculation of exciton binding energy. However, their calculations have neglected the influence of biaxial strain between the well and barriers of the QWs. In Fig. 3, we calculated the exciton transition energies for the Mg mole fraction $x = 0.12$ and $x = 0.27$ of the ZnO QWs with the effect of biaxial strain taken into consideration. The effect of overlapping between the lowest states of A1- and B1-exciton peaks, which cannot be resolved due to very close energy separation, is also considered in the calculation. Our calculations are then compared with that given in [4] and experimental result given in [2]. In our calculations, the band offset ratio and the conduction deformation potential are the adjustable parameters, which allowed to be changed in order to match with the experimental results. The values of band offset ratio and conduction deformation potential are found to

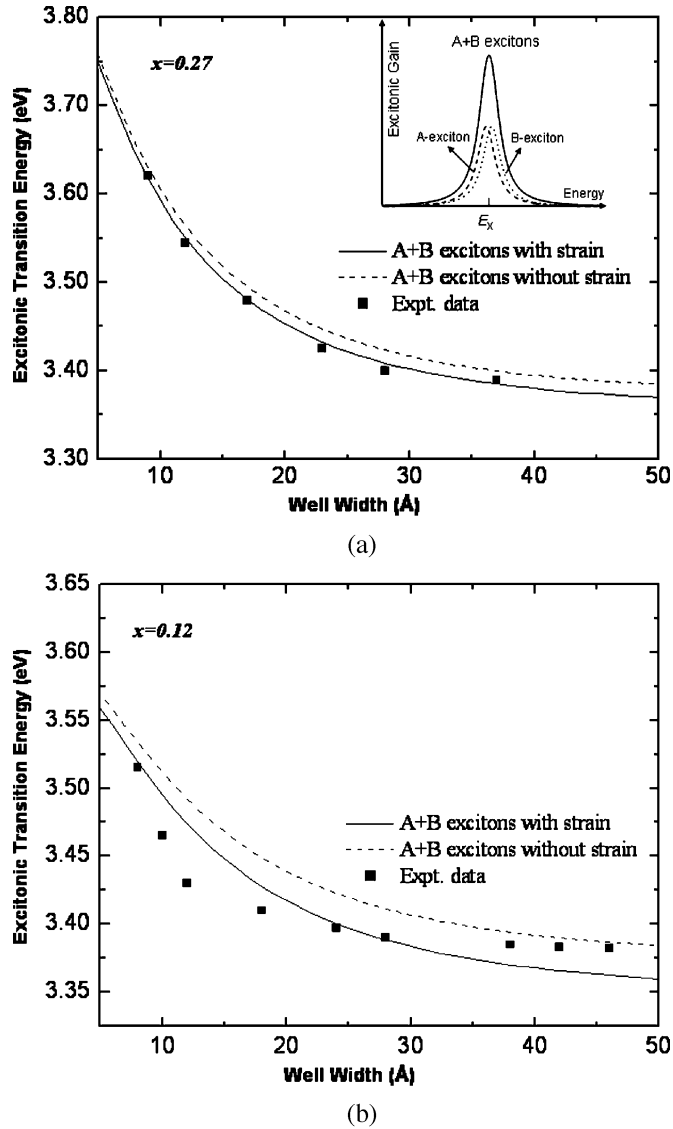


Fig. 3. Excitonic transition energy of ZnO-Mg_xZn_{1-x}O QWs for (a) $x = 0.27$ and (b) $x = 0.12$ Mg mole fraction as a function of well width. Solid (dashed) lines are the calculation with (without) the influence of biaxial strain. It is noted that the computed results of excitonic transition energy given in [4] are similar to our calculation without biaxial strain (i.e., dashed lines). Experimental data (solid squares) obtained from [2] is also plotted in the figure. The inset shows the resulting peak position as a consequence of A1- and B1-excitons overlapping.

be 60/40 and -6.8 eV, respectively, by fitting the calculated exciton transition energies to the experimental results as shown in Fig. 3. It is noted that the band offset ratio deduced from [2] is 60/40 and the conduction deformation potential recorded from ZnO nanowires is -6.05 eV [21]. This indicated that our calculation results are consistent with the available data reported in the literatures.

It is observed from Fig. 3 that the inclusion of biaxial strain, which decreases (increases) the conduction-band energy of the ZnO well (Mg_xZn_{1-x}O potential barrier) lowers the exciton transition energy in ZnO-Mg_xZn_{1-x}O QWs. In addition, the increase of well width will further decrease the energy level of the confined excitons. We have shown that the biaxial strain in the QWs affects the exciton transition energy of ZnO-Mg_xZn_{1-x}O

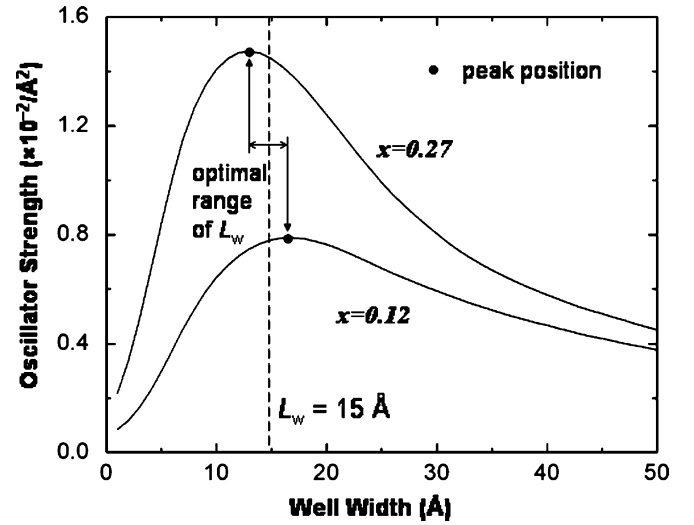


Fig. 4. Total oscillator strength of A1- and B1-excitons of ZnO-Mg_xZn_{1-x}O QWs for $x = 0.12$ and 0.27 as a function well width. The optimum value of $L_w = 15$ Å is observed for a wide range of Mg mole fraction.

QWs and, therefore, it is important to include such effects into the computation. In our model, we have ignored the influence of spontaneous and piezoelectric polarization. This is because the presence of both spontaneous and piezoelectric polarizations between the well and barriers of the ZnO-Mg_xZn_{1-x}O QWs will lead to the cancellation of internal electric field [5].

In order to deduce the optimum well width for the maximum peak gain of the ZnO-Mg_xZn_{1-x}O QWs, we calculate the corresponding oscillator strength. The oscillator strength f_X is defined as [22]

$$f_X = \frac{2}{m_0 E_X} \left| \sum_X \psi_X(\rho = 0) I_{nm} \hat{e} \cdot \mathbf{M}_{nm}(0) \right|^2. \quad (24)$$

It must be noted that due to the symmetry properties of the wurtzite ZnO crystals, A- and B-excitons transition will mainly contribute to the free-excitonic gain in TE polarization. Furthermore, the influence of C-exciton transition is ignored in our investigation, as it is far away from the valence band maximum. Therefore, only the transitions of A- and B-excitons, which are mainly of TE polarization, were taken into calculation. Fig. 4 shows the total oscillator strength per unit area of the lowest state of A1- and B1-excitons for $x = 0.12$ and $x = 0.27$ with the inclusion of biaxial strain. The optimum well width is found to be 15 Å for a wide range of Mg mole fraction. The existence of an optimum well width is attributed to the electronic confinement of excitons, which is dependant on the amount of overlapping between the electron and hole wave functions.

We also study the influence of biaxial strain on the valence band structure of the ZnO-Mg_xZn_{1-x}O QWs. The analysis of the valence bands energy dispersion for 15 Å well width and 100 Å barrier width of ZnO QWs is plotted in Fig. 5. The calculated energy dispersion for the QWs without biaxial strain effect is also included in the figure for comparison. Mole fractions of Mg with $x = 0.12$ and 0.27 , are used in the calculation. The amount of Mg in the QWs affects different potential barrier heights and

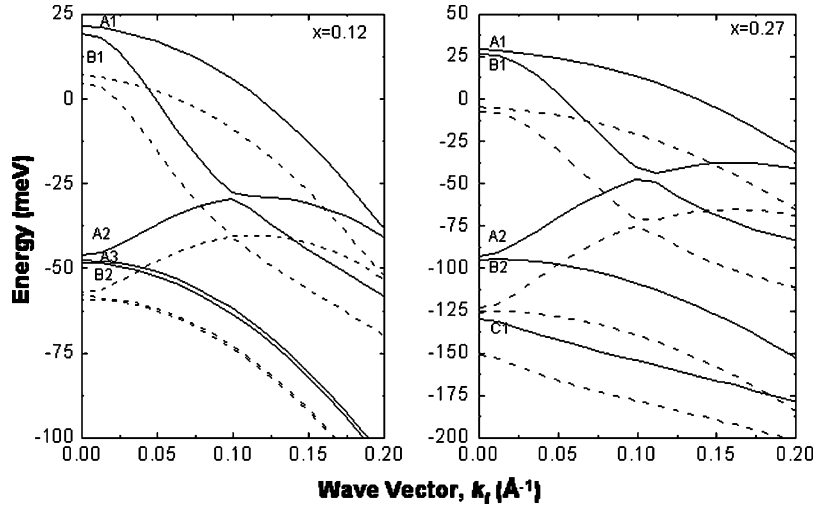


Fig. 5. Valence bands energy dispersion of 15 Å well width and 100 Å barrier width ZnO–Mg_xZn_{1–x}O QWs with $x = 0.12$ and 0.27 . Solid (dashed) lines are the calculation with (without) the influence of biaxial strain.

biaxial strains on the valence subbands. To label the subbands, we follow the bulk ZnO notation of A-, B-, and C-hole states at the Γ point with the subbands level indices, $m = 1, 2, 3, \dots$. From our calculation, it is showed that the A1 hole composition is mostly of $|u_2\rangle(|u_5\rangle)$ state (with probability >0.998) and small part of $|u_3\rangle(|u_6\rangle)$ state (with probability <0.002) for both of $x = 0.12$ and $x = 0.27$ cases. B1 is purely consist of $|u_1\rangle(|u_4\rangle)$ state at $\mathbf{k} = 0$. This composition of wavefunctions confirms that the A1- and B1-excitons are mainly TE polarized. Away from band edge, all of the states are started to overlap to form band mixing. Since the focus of the analysis is on free-excitonic band edge optical transition, the analysis is limited for the case $\mathbf{k} = 0$.

From Fig. 5, it is clearly shown that the energy different between A1- and B1- subbands (i.e., due to spin-orbit interaction) remains unchanged even the barrier energy of QWs is increased. Similar behavior is observed with the inclusion of biaxial strain [23]. This is because the effect of biaxial strain in wurtzite structure is not as pronounced as in zinc-blende crystal structure where the lower energy bands move upward. Furthermore, it is observed that A1- and B1- excitons are very close to each other such that two distinct excitonic peaks are not resolved experimentally due to small energy separation between A1- and B1-holes. This observation has verified the assumption on the overlapping of A1- and B1- excitons in the transition energy and explained the overlapping photoluminescence (PL) peaks between A1- and B1-exciton based on our spin-orbit coupling model.

Fig. 6 plots the corresponding peak free-excitonic gain versus surface carrier density for the range of x . The solid (dashed) lines represent the calculation with (without) the influence of biaxial strain taken into consideration. As expected, the ZnO–Mg_xZn_{1–x}O QWs exhibited large free-excitonic gain (in order of 10^5 cm^{-1}), which is an order higher than that of the GaN-based QWs. For $x = 0.05$, it is observed that biaxial strain has negligible effect on the peak gain due to small lattice mismatched between ZnO and Mg_xZn_{1–x}O. For $x > 0.05$, the peak gain (threshold surface carrier density) is increased (reduced) due to the presence of biaxial strain. The biaxial strain

induces the enhancement of: 1) excitonic confinement inside the QWs and 2) the density of states of the first conduction band so that the peak free-excitonic gain is improved for the increase of x . The inset of Fig. 6 shows the gain spectra versus surface carrier density of the ZnO–Mg_xZn_{1–x}O QWs with $x = 0.12$. The redshift of gain spectra indicates the importance of the consideration of the biaxial strain. The expression of Mott's density of the QWs can be written as [24]

$$n_{\text{mott}} = (\pi a_{\text{exc}}^2)^{-1} \text{ (cm}^{-2}\text{)} \quad (25)$$

where a_{exc} ($\sim 20 \text{ \AA}$) is Bohr radius of excitons. For our ZnO–Mg_xZn_{1–x}O QWs, the corresponding Mott's density is found to be $\sim 79 \times 10^{11} \text{ cm}^{-2}$, which is well above the surface carrier density used in our calculations. Hence, neglecting of electron–hole plasma recombination in the calculation of ZnO–MgZnO QWs is valid. Bandgap renormalization arisen from the many-body effects can also be ignored in our calculation due to the low surface carrier density (i.e., below the Mott's density). On the other hand, the broadening of emission linewidth, which change the shape of the Lorentzian function, can reduce the excitonic gain of the ZnO–MgZnO QWs. However, the analysis of lineshape broadening mechanism is beyond the scope of this paper.

From Fig. 6, we can approximate the low-injection free-excitonic peak gain $g (= g_b(E_X) + g_c(E_X))$ by a linear expression $g = g_N(N - N_o)$, where g_N is defined as differential gain constant, N is the injected surface carrier density, and N_o is the surface carrier density at transparency. Fig. 7 plots the dependence of g_N and N_o on the value of x for the ZnO–Mg_xZn_{1–x}O QWs with $L_w = 15 \text{ \AA}$. The value of g_N (N_o) increases (decreases) with increasing values of x and saturates for $x > 0.27$. Increasing values of x improve the electronic confinement due to greater potential barrier. However, the enhancement of electronic confinement becomes saturated for $x > 0.27$, therefore, this causes the saturation of the free-excitonic gain.

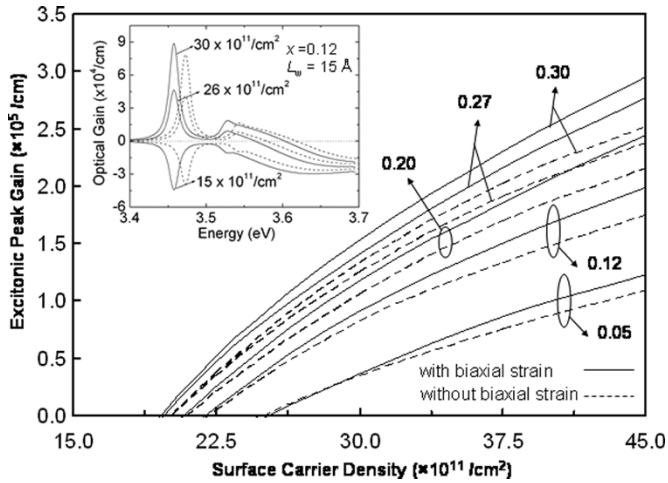


Fig. 6. Peak free-excitonic gain versus surface carrier density of $\text{ZnO-Mg}_x\text{Zn}_{1-x}\text{O}$ QWs for x varies from 0.05 to 0.30 and $L_w = 15 \text{ \AA}$. Solid (dashed) lines are the calculation with (without) the influence of biaxial strain. The inset shows the gain spectra versus surface carrier density of the $\text{ZnO-Mg}_x\text{Zn}_{1-x}\text{O}$ QWs with $x = 0.12$ and $L_w = 15 \text{ \AA}$.

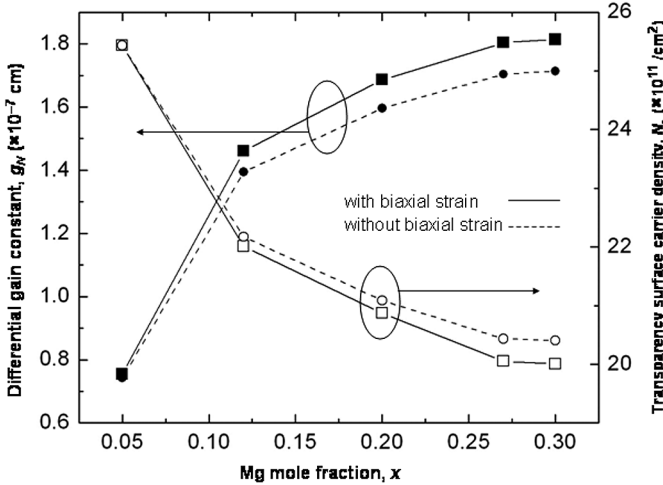


Fig. 7. Dependence of differential gain constant, g_N and transparency surface carrier density, N_o , of $\text{ZnO-Mg}_x\text{Zn}_{1-x}\text{O}$ QWs with $L_w = 15 \text{ \AA}$ versus the mole fraction of Mg. Solid (dashed) lines are the calculation with (without) the influence of biaxial strain.

IV. CONCLUSION

In conclusion, we have investigated the free-excitonic gain of $\text{ZnO-Mg}_x\text{Zn}_{1-x}\text{O}$ QWs theoretically. The influence of biaxial strain and exciton-phonon interaction was taken into consideration. The band offset ratio and conduction band deformation potential were also extracted from the experimental data. Hence, the influence of biaxial strain on the peak free-excitonic gain of $\text{ZnO-Mg}_x\text{Zn}_{1-x}\text{O}$ QWs was investigated. It is found that the free-excitonic gain can be maximized for x varies between 0.27 and 0.30 if well width is chosen to be 15 \AA . For $x > 0.30$, $\text{Mg}_x\text{Zn}_{1-x}\text{O}$ will change phase to cubic structure so that the value of x larger than 0.30 is not considered.

REFERENCES

[1] H. D. Sun, T. Makino, Y. Segawa, M. Kawasaki, A. Ohtomo, K. Tamura, and H. Koinuma, "Enhancement of exciton binding energies in ZnO/ZnMgO multiquantum wells," *J. Appl. Phys.*, vol. 91, pp. 1993–1997, 2002.

[2] T. Makino, C. H. Chia, N. T. Tuan, H. D. Sun, Y. Segawa, M. Kawasaki, A. Ohtomo, K. Tamura, and H. Koinuma, "Room-temperature luminescence of excitons in $\text{ZnO}/(\text{Mg}, \text{Zn})\text{O}$ multiple quantum wells on lattice-matched substrates," *Appl. Phys. Lett.*, vol. 77, pp. 975–977, 2000.

[3] J. Pollmann and H. Büttner, "Effective Hamiltonians and binding energies of Wannier excitons in polar semiconductors," *Phys. Rev. B*, vol. 16, pp. 4480–4490, 1977.

[4] G. Coli and K. K. Bajaj, "Excitonic transitions in ZnO-MgZnO quantum well heterostructures," *Appl. Phys. Lett.*, vol. 78, pp. 2861–2863, 2001.

[5] S. H. Park and D. Ahn, "Spontaneous and piezoelectric polarization effects in wurtzite ZnO-MgZnO quantum well lasers," *Appl. Phys. Lett.*, vol. 87, p. 253 509, 2005.

[6] D. Ahn, S. H. Park, E. H. Park, and T. K. Yoo, "Optical gain and luminescence of a ZnO-MgZnO quantum well," *IEEE Photon. Technol. Lett.*, vol. 18, no. 2, pp. 349–351, Jan. 2006.

[7] W. J. Fan, M. F. Li, T. C. Chong, and J. B. Xia, "Valence hole subbands and optical gain spectra of $\text{GaN}/\text{Ga}_{1-x}\text{Al}_x\text{N}$ strained quantum wells," *J. Appl. Phys.*, vol. 80, pp. 3471–3478, 1996.

[8] W. R. L. Lambrecht, A. V. Rodina, S. Limpijumngong, B. Segall, and B. K. Meyer, "Valence-band ordering and magneto-optic exciton fine structure in ZnO ," *Phys. Rev. B*, vol. 65, pp. 075 207 01–075 207 12, 2002.

[9] Y. C. Yeo, T. C. Chong, M. F. Li, and W. J. Fan, "Electronic band structures and optical gain spectra of strained wurtzite $\text{GaN-Al}_x\text{Ga}_{1-x}\text{N}$ quantum well lasers," *IEEE J. Quantum Electron.*, vol. 34, no. 3, pp. 526–534, Mar. 1998.

[10] S. L. Chuang and C. S. Chang, "k.p method for strained wurtzite semiconductors," *Phys. Rev. B*, vol. 54, pp. 2491–2504, 1996.

[11] R. S. Zheng and M. Matsuura, "Exciton binding energies in polar quantum wells with finite potential barriers," *Phys. Rev. B*, vol. 58, pp. 10 769–10 777, 1998.

[12] N. Mori and T. Ando, "Electron-optical-phonon interaction in single and double heterostructures," *Phys. Rev. B*, vol. 40, pp. 6175–6188, 1989.

[13] L. F. Register, "Microscopic basis for a sum-rule for polar-optical-phonon scattering of carriers in heterostructures," *Phys. Rev. B*, vol. 45, pp. 8756–8759, 1992.

[14] P. J. Mares and S. L. Chuang, "Modeling of self-electro-optic-effect devices," *J. Appl. Phys.*, vol. 74, pp. 1388–1397, 1993.

[15] S. L. Chuang, S. Schmittrink, D. A. B. Miller, and D. S. Chemla, "Exciton Greens-function approach to optical-absorption in a quantum well with an applied electric field," *Phys. Rev. B*, vol. 43, pp. 1500–1509, 1991.

[16] Y. C. Yeo, T. C. Chong, and M. F. Li, "Electronic band structures and effective-mass parameters of wurtzite GaN and InN ," *J. Appl. Phys.*, vol. 83, pp. 1429–1436, 1998.

[17] H. D. Li, S. F. Yu, A. P. Abiyasa, C. Yuen, S. P. Lau, H. Y. Yang, and S. P. Leong, "Strain dependence of lasing mechanisms in ZnO epilayers," *Appl. Phys. Lett.*, vol. 86, p. 261 111, 2005.

[18] S. L. Chuang, *Physics of Optoelectronic Devices*. New York: Wiley, 1995.

[19] F. Jain and W. Huang, "Modeling of optical gain in InGaN-AlGaIn and $\text{In}_x\text{Ga}_{1-x}\text{N-In}_y\text{Ga}_{1-y}\text{N}$ quantum-well lasers," *IEEE J. Quantum Electron.*, vol. 32, no. 5, pp. 859–864, May 1996.

[20] D. G. Thomas, "The exciton spectrum of zinc oxide," *J. Phys. Chem.*, vol. 15, pp. 86–96, 1960.

[21] W. Shan, W. Walukiewicz, J. W. Ager, K. M. Yu, Y. Zhang, S. S. Mao, R. Kling, C. Kirchner, and A. Waag, "Pressure-dependent photoluminescence study of ZnO nanowires," *Appl. Phys. Lett.*, vol. 86, p. 153 117, 2005.

[22] C. Y. P. Chao and S. L. Chuang, "Momentum space solution of exciton excited-states and heavy-hole light-hole mixing in quantum wells," *Phys. Rev. B*, vol. 48, pp. 8210–8221, 1993.

[23] M. Suzuki and T. Uenoyama, "Strain effect on electronic and optical properties of GaN/AlGaIn quantum-well lasers," *J. Appl. Phys.*, vol. 80, pp. 6868–6874, 1996.

[24] S. L. Chuang, "Optical gain of strained wurtzite GaN quantum well lasers," *IEEE J. Quantum Electron.*, vol. 32, no. 10, pp. 1791–1800, Oct. 1996.

[25] A. Ohtomo, M. Kawasaki, I. Ohkubo, H. Koinuma, T. Yasuda, and Y. Segawa, "Structure and optical properties of $\text{ZnO-Mg}_{0.2}\text{Zn}_{0.8}\text{O}$ superlattices," *Appl. Phys. Lett.*, vol. 75, pp. 980–982, 1999.

[26] A. Ohtomo, M. Kawasaki, T. Koida, K. Masubuchi, H. Koinuma, Y. Sakurai, Y. Yoshida, T. Yasuda, and Y. Segawa, " $\text{Mg}_x\text{Zn}_{1-x}\text{O}$ as a II–VI widegap semiconductor alloy," *Appl. Phys. Lett.*, vol. 72, pp. 2466–2468, 1998.

- [27] J. E. Rowe, M. Cardona, and F. H. Pollak, "Valence band symmetry and deformation potentials of ZnO," *Solid State Commun.*, vol. 6, pp. 239–242, 1968.
- [28] Landolt-Bornstein, *Numerical Data and Functional Relationship in Science and Technology*. Berlin, Germany: Springer-Verlag, 1982, vol. 17, p. 35.

A. P. Abiyasa received the B.Eng degree in electrical and electronic engineering from Nanyang Technological University, Singapore, in 2004, where he is currently working toward the Ph.D. degree.

His research interests are the design and fabrication of ultraviolet light-emitting devices and lasers using wide bandgap semiconductor materials.

S. F. Yu (M'03–SM'03) received the B.Eng degree from University College, London University, London, U.K., in 1990 and the D.Phil. degree from Robinson College, Cambridge University, Cambridge, U.K., in 1993.

Currently, he is an Associate Professor and Program Director in the School of Electrical and Electronic Engineering, Nanyang Technological University, Singapore. He is also a Cluster Manager at NanoCluster Headquarter, Research TechnoPlaza, Nanyang Technological University, Singapore. His main research interest includes the fundamental study, design, and optimization of semiconductor lasers including distributed feedback lasers and vertical-cavity surface-emitting lasers.

W. J. Fan received the B.Eng. degree in applied physics from National University of Defense Technology, Changsha, China, in 1987, the M.Sc degree from Institute of Semiconductor, Chinese Academy of Science, Beijing, China, in 1990, and the Ph.D. degree in electrical engineering from the National University of Singapore, Singapore, in 1997.

Presently, he is an Associate Professor at Nanyang Technological University, Singapore.

S. P. Lau received the B.Sc. degree from North London University, London, U.K., and the Ph.D. degree from the University of Wales, Swansea, U.K.

He is an Associate Processor in the School of Electrical and Electronic Engineering in the Nanyang Technological University (NTU), Singapore. Before joining NTU, he worked in the University of Surrey and the University of Wales Swansea as a Research Fellow and Senior Research Assistant, respectively. He has published over 120 papers in refereed international journals and received several invited oral presentations at various international conferences. He was also the chairman of the Symposium N: ZnO and Related Materials, 3rd International Conference on Materials for Advanced Technologies (ICMAT) held in Singapore in 2005.